Strong Broadband Terahertz Optical Activity through Control of the Blaschke Phase with Chiral Metasurfaces

Michael A. Cole,[1,*] Wen-chen Chen,[2] Mingkai Liu,[1] Sergey S. Kruk,[1] Willie J. Padilla,[3] Ilya V. Shadrivov,[1] and David A. Powell[1]

[1]*Nonlinear Physics Centre and Centre for Ultrahigh Bandwidth Devices for Optical Systems, Research School of Physics and Engineering, The Australian National University, Canberra, Australian Capital Territory 2601, Australia*

[2]*Computer Simulation Technology (CST), San Mateo, California 94404, USA*

[3]*Department of Electrical and Computer Engineering, Duke University, Durham, North Carolina 27708, USA*

(Received 12 January 2017; revised manuscript received 15 June 2017; published 21 July 2017)

We demonstrate terahertz chiral metamaterials that achieve resonant transmission and strong optical activity. This response is realized in a metasurface coupled to its Babinet complement, with additional twist. Uniquely, the optical activity achieved in this type of metamaterial is weakly dispersive around the resonant transmission maxima, but it can be highly dispersive around the transmission minima. It has recently been shown that this unique optical activity response is closely related to zeros in the transmission spectra of circular polarizations through the Kramers-Kronig relations and strong resonant features in the optical activity spectrum corresponding to the Blaschke phase terms. Here we demonstrate how modifying the meta-atom geometry greatly affects the location and magnitude of these Blaschke phase terms. We study three different meta-atoms, which are variations on the simple cross structure. Their responses are measured using terahertz time-domain spectroscopy and analyzed via numerical simulations.

DOI: 10.1103/PhysRevApplied.8.014019

I. INTRODUCTION

A chiral metamaterial is a structure that cannot be superimposed onto its mirror image; these structures are said to have "handedness". The main feature of a chiral material is that it breaks the degeneracy between right-circularly-polarized (RCP) and left-circularly-polarized (LCP) electromagnetic waves. This results in a phase difference between the RCP and LCP waves transmitted through the structure. An incident linearly polarized wave can be decomposed into LCP and RCP waves, and any difference in phase will result in rotation of the plane of polarization. Since chiral structures couple electric and magnetic fields, they are often implemented in complex geometries such as spirals [1] or metafoils [2], which can achieve carefully balanced responses to the two fields [3]. However, such structures require complex three-dimensional fabrication techniques, which in many cases are not practical [4].

Scalable designs which can be readily implemented at shorter wavelengths are often based on bilayered metallic structures separated by a dielectric layer [5–18]. Each layer in the structure is typically treated as an array of dipoles, with the coupled layers supporting symmetric and antisymmetric modes. Introducing twist between the layers couples these modes and leads to optical manifestations of chirality [7,12–16,19,20].

The main limitation of these coupled metallic dipole-type structures is the unfavorable trade-off between the strength of polarization rotation, the transmission magnitude, and the usable operating bandwidth [21]. It has been demonstrated in the microwave frequency range [8,9,21] that combining a meta-atom with its Babinet complement, twisted through some angle, leads to polarization rotation which is strong but nonresonant in the vicinity of the transmission resonance. It was recently shown that the resonances of optical activity in low-loss structures can be well explained through the appearance of Blaschke phase terms for only one circular polarization [21]. These terms were introduced as correction terms required when using the Kramers-Kronig relations between the optical activity and circular dichroism spectra [22]. Intuitively, they can be understood in the limit of a lossless structure, where circular dichroism goes to zero yet optical activity remains finite. Since the Kramers-Kronig relations predict zero optical activity in this case, the Blaschke terms account for the finite optical activity.

In this work, we demonstrate that large polarization rotation can also be achieved and increased not by changing the thickness of the dielectric layer, but instead, by changing the geometry of the structures themselves. We fabricate three bilayer metallic structures and test them both experimentally and numerically in the terahertz regime. The structures are referred to as the crosses, arrows, and arcs; microscope images of the fabricated structures can be seen in Figs. 1(a)–1(c), 1(d)–1(f), and 1(g)–1(i), respectively. Furthermore, we present a numerical analysis of the structures using CST

*michael.cole@anu.edu.au

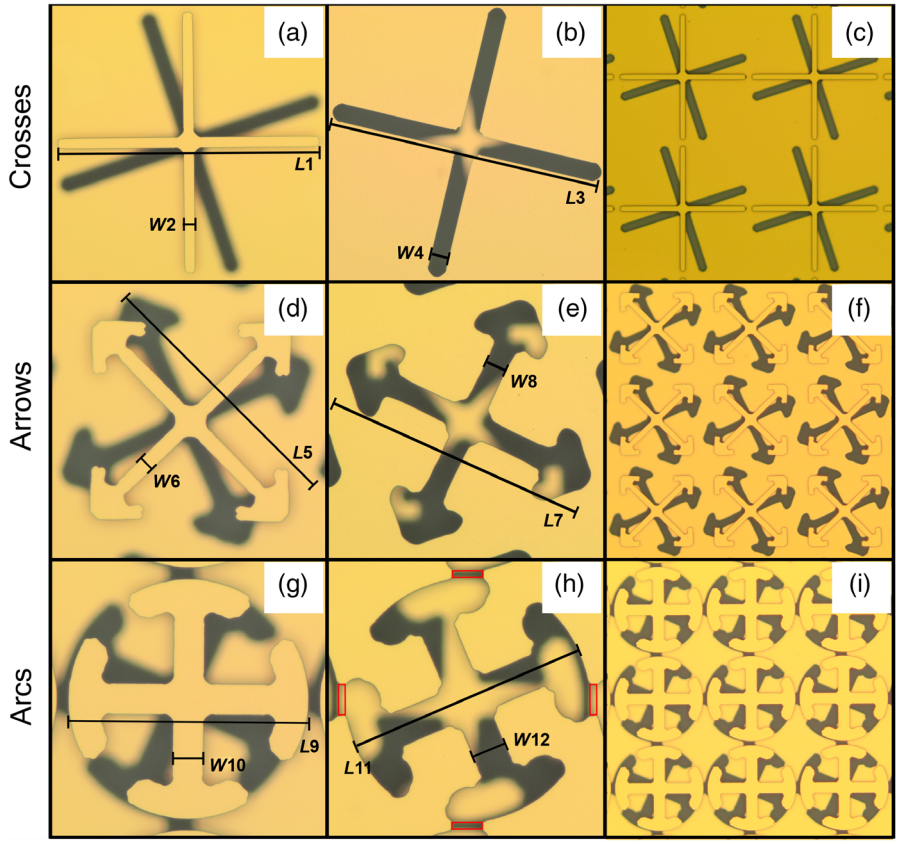

FIG. 1. Panels (a),(b) show microscope pictures of the two sides of the unit cell of the cross structure, panels (d),(e) the two sides of the arrows structure, and panels (g),(h) the two sides of the arcs structure. It can be seen that the two structures are not perfect complementary structures of one another due to fabrication errors. The red rectangles in (h) indicate the "bleeding together" of the complementary patterns, which contributes to significant fluctuations in the terahertz signal. Panels (c),(f),(i) show a portion of the lattice for each structure.

Microwave Studio to show that by changing the geometry of the structure, we can move the complex zeros in the transmission to increase the polarization rotation. Then we establish that the Kramers-Kronig relations for the numerical circular dichroism and optical activity are in agreement when we account for the Blaschke phase terms as shown in Ref. [22]. Finally, we analyze the contributions to the optical activity from the Blaschke phase terms as well as the Kramers-Kronig relations for each structure.

II. THEORETICAL BACKGROUND

A. The measured quantities

The quantities of interest for the experimental analysis of this work are the transmission T, optical activity Φ, and ellipticity η of the terahertz signal. Ideally, our structure has high transmission, low ellipticity, and large flat optical activity at the operational frequency. The measured transmission coefficients for our structure are the normalized signals of T_{xx}, T_{yy}, T_{xy}, and T_{yx}. From these quantities obtained through simulation and terahertz time-domain spectroscopy (THz TDS), we are able to calculate the transmission for the right and left circular polarizations as

$$T_{\pm\pm} = \frac{1}{2}[T_{xx} + T_{yy} \pm i(T_{xy} - T_{yx})]. \tag{1}$$

Following the above results, the ellipticity of the transmitted wave (assuming an incident linearly polarized wave) can be calculated as

$$\eta = \frac{1}{2}\arctan\left[\frac{|T_{++}|^2 - |T_{--}|^2}{|T_{++}|^2 + |T_{--}|^2}\right]. \tag{2}$$

Finally, the optical activity can be found by

$$\Phi = \frac{1}{2}\arg\frac{T_{++}}{T_{--}}. \tag{3}$$

B. Kramers-Kronig relations for optical activity

The Kramers-Kronig relations are a fundamental concept for many physical phenomena and are a bridge between the real and imaginary parts of an analytic complex function [22,23]. The Kramers-Kronig relations are typically used in reflectivity, dielectric functions, and index of refraction calculations [23]. These relations can also relate the logarithm of the complex transmission coefficient to the frequency-dependent phase as shown, e.g., in Ref. [22].

Once we calculate or measure the transmission coefficients, the Kramers-Kronig relations predict that the optical activity will have the value $\hat{\Phi}_{\mathrm{KK}}$,

$$\hat{\Phi}_{\mathrm{KK}}(\omega) = \frac{\omega}{\pi} P \int_0^\infty \ln\left|\frac{T_{++}(\omega')}{T_{--}(\omega')}\right| \frac{d\omega'}{\omega'^2 - \omega^2}, \tag{4}$$

based on the assumption that the integrand is an analytical function. However, this assumption is violated if $|T_{++}(\omega')| = 0$ or $|T_{--}(\omega')| = 0$ for any complex ω' in the upper half of the complex plane using the time

convention $t(\omega) = |t(\omega)| \exp[i\Psi(\omega)]$ [22]. In such cases, the optical activity must be supplemented with an additional Blaschke term Φ_B. This additional Blaschke phase term is a series [22] given by

$$\Phi_B = \frac{1}{2}\sum_{i=1}^{n_+} \arg\left(\frac{\omega-\omega_{+i}}{\omega-\omega_{+i}^*}\right) - \frac{1}{2}\sum_{i=1}^{n_-} \arg\left(\frac{\omega-\omega_{-i}}{\omega-\omega_{-i}^*}\right), \quad (5)$$

where $\omega_{\pm i}$ are the complex frequencies of the zeros in transmission for each circular polarization satisfying $|T_{++}(\omega_{+i})| = 0$ and $|T_{--}(\omega_{-i})| = 0$. The symbol * indicates complex conjugation. The upper limits on the summations $n_\pm$ are the number of terms in the Blaschke phase for each polarization.

In practice, Φ_{KK} must be calculated from simulated or measured data obtained over a finite bandwidth. This means that the obtained value of Φ_{KK} is only an estimate; hence, the corresponding total optical activity is denoted Φ_E to indicate that it is an estimate of Φ:

$$\Phi_E = \hat{\Phi}_{KK}(\omega) - \Phi_B. \quad (6)$$

In the limiting case that Eq. (4) is calculated over an infinite frequency range, Φ_E should converge to Φ.

In the case of lossless media with rotational symmetry C_N, $(N > 2)$, $|T_{++}(\omega)| = |T_{--}(\omega)|$, and from Eq. (4), this scenario leads to $\hat{\Phi}_{KK}(\omega) = 0$. In such cases, only the Blaschke phase contributes to the optical activity, and in the low-loss structures considered here, we expect it to be dominant. Therefore, structural variations which change the location and magnitude of these Blaschke phase contributions lead to significant changes of the optical activity.

III. CONTROL OF BLASCHKE PHASE BY METASURFACE GEOMETRY

We design three structures to study how the optical activity and Blaschke phase are related and how they evolve with respect to changes in geometry. The first of the three designs is a metasurface of simple crosses and their complements separated by a dielectric layer, as shown in Figs. 1(a)–1(c). By increasing the complexity of the structure slightly, the second structure is an array of crossed double-sided arrows and their complements shown in Figs. 1(d)–1(f). The final structure replaced the arrowheads with circular arcs as seen in Figs. 1(g)–1(i). All of the structures are designed to give high transmission at the second resonance of the structure, and all dimensions are optimized to achieve this. The structures are also chosen to yield low ellipticity and, most important, large optical activity at maximum transmission.

The measured dimensions of the structures labeled in Fig. 1 are given in Table I along with the ideal dimensions of the structures as specified in the design. The thickness of all the gold layers for each structure is 0.2 μm. The gold layers of all the structures are separated by a layer of benzocyclobutene (BCB), with additional top and bottom layers to embed the structure for protection during fabrication, and each layer of BCB is approximately 6 μm. Ideally, the single elements have identical dimensions to their complements; however, the fabricated samples have imperfections, and the dimensions differ slightly between the two layers. For the simulations performed in this section, we use the ideal dimensions from Table I.

TABLE I. Dimensions of the fabricated layers (element and complement) pictured in Fig. 1 and the ideal simulated structures used in our numerical analysis. Ideally, the dimensions of the two layers are identical.

Structure	Figure 1 reference	Length (μm)	Width (μm)
Ideal crosses		153.6	6.6
Crosses	$L1$, $W2$	153.6	6.6
Complementary crosses	$L3$, $W4$	159.2	11.6
Ideal arrows		99.0	6.0
Arrows	$L5$, $W6$	105.0	5.5
Complementary arrows	$L7$, $W8$	106.8	8.8
Ideal arcs		89.7	12.9
Gold thickness		0.2	
BCB thickness		6.0	

We present the numerically simulated transmission spectra for each structure on a decibel scale in Figs. 2(a), 2(d), and 2(g), for both right (black) and left (red) circular polarizations. It can be seen that the left- and right-handed spectra are almost identical, except in the vicinity of transmission minima. In Figs. 2(b), 2(e), and 2(h), the corresponding optical activity for each structure is shown by the black curves. For comparison purposes, we show the reconstruction of this optical activity (Φ_E) including both terms from the right-hand side of Eq. (6) in red. The Kramers-Kronig integral in Eq. (4) is calculated numerically over the frequency range of the simulated results. The singular part of the principal-value integral is subtracted and handled analytically, similar to Ref. [24]. The Blaschke terms are fitted manually to achieve good agreement with the calculated optical activity (Φ). In Figs. 2(c), 2(f), and 2(i), we show separately the contributions to the optical activity of each term from Eq. (5) and the Kramers-Kronig term from Eq. (4). The first term in the right circular polarization of the Blaschke phase (Φ_{B+1}) is shown by the black curve, and the second term for this polarization (Φ_{B+2}) is shown in blue (note that the second Blaschke term for the RCP occurs only in the arc structure within our frequency range). The first term in the left circular polarization (Φ_{B-1}) is shown in red. The final contribution to the reconstructed optical activity shown in Figs. 2(b), 2(e), and 2(h) (red) is the $\hat{\Phi}_{KK}$, which is shown by the green curve in Figs. 2(c), 2(f), and 2(i).

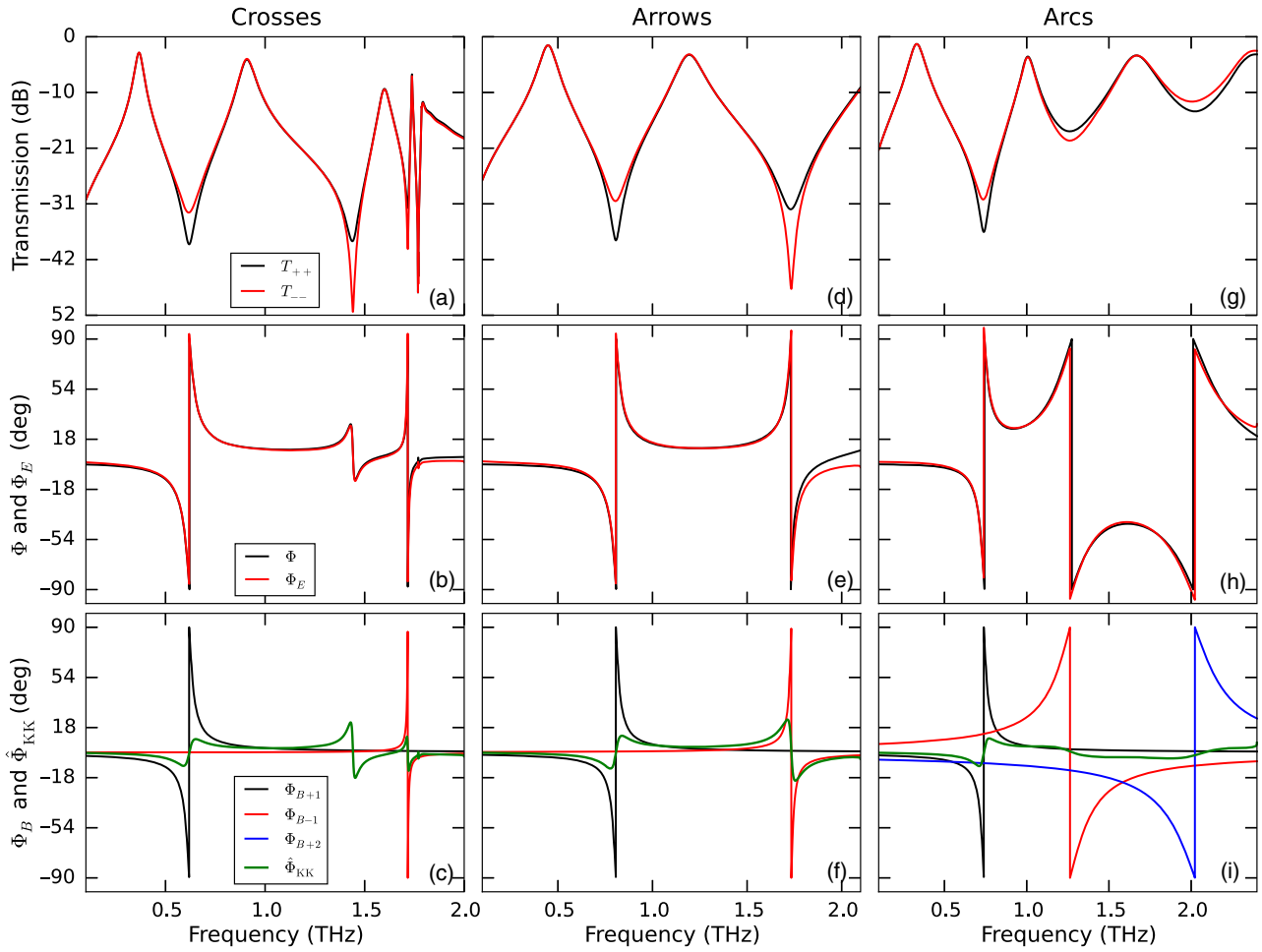

FIG. 2. Panels (a),(d),(g) show the transmission on a decibel scale for each structure. The black curves show the T_{++} modes, and the red curves show the T_{--} modes. Panels (b),(e),(h) show the optical activity (Φ, black curves), and the red curves ($\Phi_E = \hat{\Phi}_{KK}$-Φ_B) show the fitted curves composed of the Kramers-Kronig and Blaschke phase terms. Finally, panels (c),(f),(i) show the Φ_{B+1} term (black curves) for the T_{++} mode, the red curves show the Φ_{B-1} term for the T_{--} mode, and the blue curve in panel (i) shows the Φ_{B+2} term for the second Blaschke term in the T_{++} mode of the arcs structure. The green curves show the contribution from the Kramers-Kronig relations in each structure.

Examining Figs. 2(c), 2(f), and 2(i), it can be seen that the component $\hat{\Phi}_{KK}$ related by the Kramers-Kronig transformation to the circular dichroism is the lowest contributor to the optical activity. Near resonances, we expect stronger local currents and fields, hence, larger differences in losses between the two circular polarizations leading to the observed higher circular dichroism. This effect yields a larger phase contribution given by the Kramers-Kronig relations and added influence on the optical activity. More significantly, we show that the Blaschke phase plays a dominant role in the strength of the optical activity of the structure. There are two significant ways that the geometry influences the Blaschke phase contributions to optical activity: (1) As the real parts of the zero frequencies approach each other, there is an increase in optical activity with a clear trade-off in bandwidth, as seen in Figs. 2(b), 2(e), and 2(h). (2) For each complex frequency with zero transmission, there is a greater contribution to optical activity if it has a larger imaginary part.

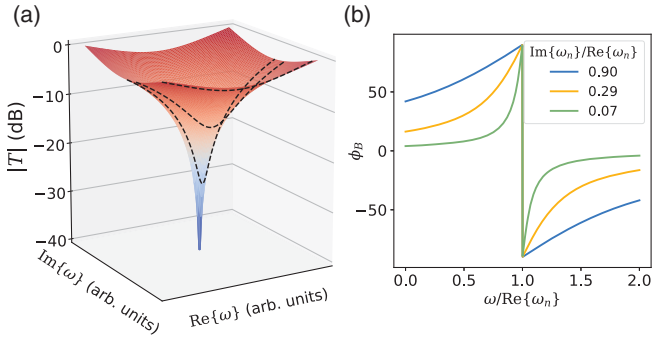

FIG. 3. (a) Schematic of transmission spectrum in the complex frequency plane in the vicinity of a zero. Dashed lines show the transmission curves corresponding to different imaginary parts of the zero frequency. (b) Blaschke phase terms corresponding to each of the dashed lines in panel (a), showing that a larger imaginary part of $\omega_{\pm i}$ leads to a larger bandwidth of significant optical activity.

To clarify the role of zeros at complex frequencies, we include a schematic in Fig. 3(a) illustrating the transmission on a decibel scale in the vicinity of a zero. The dashed curves show how the observed transmission response changes in character depending on how close the complex zero is to the real frequency axis. The dip becomes shallower as the complex zero of transmission moves away from the real frequency axis. Figure 3(b) shows the corresponding Blaschke phase terms. Examination of Eq. (5) shows that each Blaschke term has a pair of branch points at $\omega_{\pm i}$ and $\omega^*_{\pm i}$. This always leads to a jump in phase of 180° as the real frequency axis passes through the branch cut. However, the influence of this term at other frequencies depends strongly on the imaginary part of $\omega_{\pm i}$. It can be seen in Fig. 3(b) that as the imaginary part of the zero frequency increases from 0.07 to 0.9 (normalized to the real part), the optical activity becomes significant over a wider bandwidth. This agrees with Figs. 2(a), 2(d), and 2(g), where the sharper transmission minima are associated with zeros close to the real axis; hence, the corresponding Blaschke phase terms are quite narrow band and decay quickly at frequencies away from the zero. On the other hand, the weak transmission minima shown in Fig. 2(g) give very broad Blaschke phase contributions, which can contribute to optical activity over a broad frequency range. Hence, the arc structure has the largest optical activity in simulation.

IV. FABRICATION AND MEASUREMENTS

Each of the structures are fabricated by spin-coating resist, UV photolithography, and *e*-beam evaporation of the gold layers, with the results shown in Fig. 1. The designs specify identical dimensions for the positive elements and their complements; however, slight differences in development of the exposed photoresist and variations in the lift-off of the complementary patterns produced slight deviations in the dimensions of the structures. These aberrations can be seen in the recorded dimensions in Table I and Fig. 1.

All THz TDS measurements are taken in transmission mode in a nitrogen atmosphere with terahertz polarizers located in the signal path symmetrically on each side of the sample. Reference signals for each polarization T_{xx} and T_{yy} are taken in free space without the sample, as detailed in the Supplemental Material [25]. The polarizers are positioned at the coplanar positions of +45° and −45° to the polarization of the terahertz source for the T_{xx} and T_{yy} reference signals, respectively. The sample is inserted and four measurements are taken by manually rotating the polarizers to obtain the T_{xx}, T_{yy}, T_{xy}, and T_{yx} measurements. The normalized spectra are then used in Eqs. (1)–(3) to obtain the transmission for each polarization T_{++}, T_{--}, optical activity (Φ), and ellipticity (η). Because of symmetry, we expect no cross-coupling between left- and right-circularly-polarized waves. Experimentally, we confirm that these cross-coupling terms T_{+-} and T_{-+} are less than 0.18 over the measured frequency range, as shown in the Supplemental Material [25].

V. RESULTS AND DISCUSSION

To enable comparison with the measured results, the simulation results presented in this section are based on the experimentally measured dimensions presented in Table I. For the arc structure, the defects outlined in red in Fig. 1(h) are also included in these simulations.

A. Crosses

The transmission of the cross structure is optimized in simulations to give the highest transmission for the second resonance frequency of the structure at 0.93 THz. Figures 4(a) and 4(b) show the transmission for the right- and left-handed polarizations from the cross structure, respectively. The maximum transmission amplitude at the second resonance for the $|T_{++}|$ polarization has a simulated value of 0.75 and an experimental value of 0.65. The peaks of the experimental data are blueshifted slightly by approximately 0.05 THz for both the left and right polarizations. Figure 4(c) shows the low ellipticity (−1.7°) of the terahertz signal at 0.93 THz compared to a simulated value of 0.14°. Finally, the optical activity shown in Fig. 4(d) remains nearly flat throughout the frequency band of the second resonance with an experimental rotation of about 8.4° and a simulated optical activity of 8.8° at 0.93 THz.

B. Arrows

Adding some complexity to the cross structure offers the possibility for higher polarization rotation. By altering the

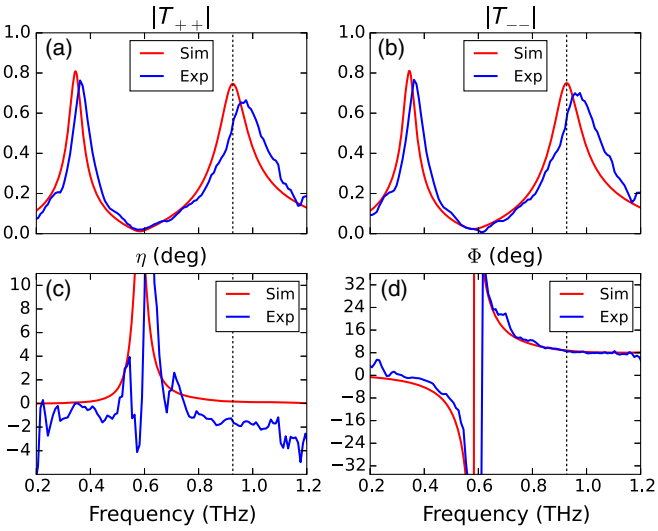

FIG. 4. Results for the crosses depicted in Figs. 1(a)–1(c). Numerical results are shown in red, and the experimental THz TDS measurements are shown in blue. Transmission $|T_{++}|$ and $|T_{--}|$ (a),(b) and ellipticity of the terahertz waves (c) remains close to zero except near the transmission minimum. Panel (d) shows the optical activity of approximately 8.4° at our simulated operational frequency of 0.93 THz indicated by the black dashed line at the second resonance in the crosses structure.

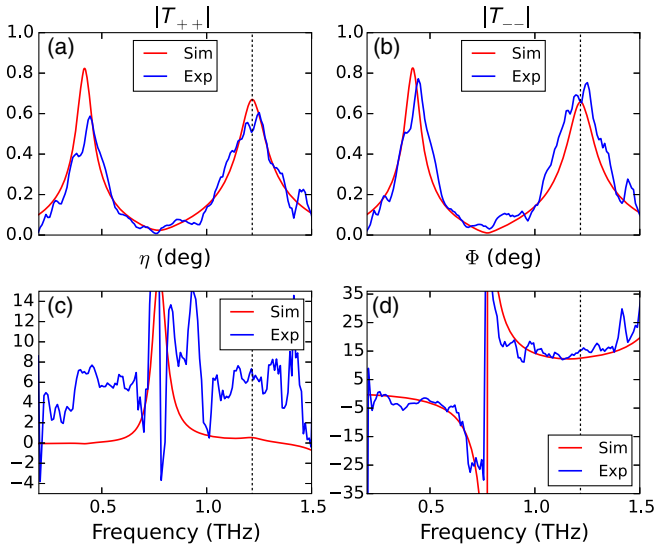

FIG. 5. Results for the arrows depicted in Figs. 1(d)–1(f). Numerical results are shown in red, and the experimental THz TDS measurements are shown in blue. Transmission $|T_{++}|$ and $|T_{--}|$ (a),(b) and ellipticity of the terahertz waves (c). Panel (d) shows the optical activity of approximately 12.5° at our operational frequency of 1.2 THz indicated by the black dashed line at the second resonance in the arrows structure.

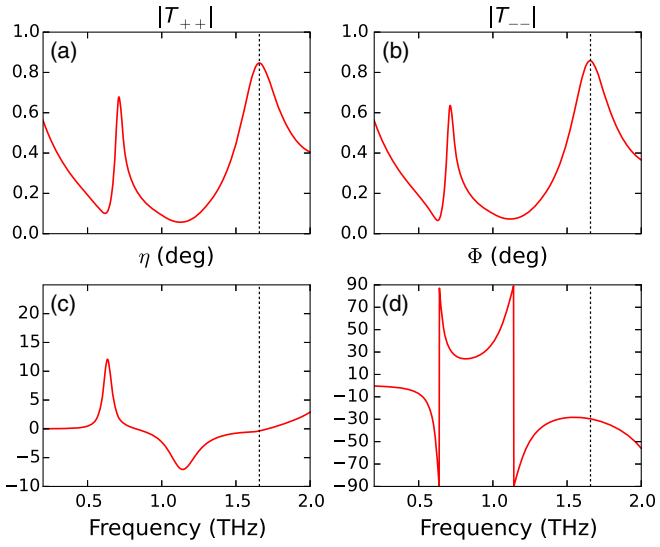

FIG. 6. Results for the arcs depicted in Figs. 1(g)–1(i). Numerical results are shown in red. Transmission $|T_{++}|$ and $|T_{--}|$ (a),(b) and ellipticity of the terahertz waves (c). Panel (d) shows the optical activity of approximately 30.0° at our operational frequency of 1.7 THz indicated by the black dashed line at the second resonance in the arcs structure.

structure, we also lower the transmission of the terahertz signal to a value of approximately 0.67 in the CST simulations with experimental values of 0.56 for the $|T_{++}|$ and 0.70 for the $|T_{--}|$ transmission shown in Figs. 5(a) and 5(b). Figure 5(c) shows the ellipticity of the terahertz signal, which is significantly higher than the cross structure, especially when compared to the predicted simulation values which are low at the operational frequency of 1.2 THz. The ellipticity at the second resonance is 6.3°, whereas the simulated value is 0.5°. The arrows structure does indeed have higher optical activity when compared to the crosses structure shown in Fig. 4(d). The optical activity again remains relatively flat over the second resonance band of the design with a simulated value of 12.5° compared to an experimental value of 15.3°.

C. Arcs

The simulated results for the arc structure are shown in Fig. 6. Unfortunately, the fabrication of the arc structures is unsuccessful, and, therefore, the corresponding experimental results are presented only in the Supplemental Material [25]. However, the simulated results of the experimentally accurate structures are presented here to demonstrate the overall message of our work. Furthermore, the level of optical activity is compelling, and it can be realized with a more accurate fabrication procedure. The simulated transmission of the structure has an approximate value of 0.80 at the operational frequency of our structure, 1.7 THz. The optical activity has a simulated value of 29.8°.

D. Results summary

Table II clarifies and compares the results of the optical activity for the crosses and arrows structures, the simulated ideal structures presented in Fig. 2, and the results of the realistic simulated structures presented in this section. From the values in Table II, it can be seen that for even slight changes in the geometry of the structure, the optical activity is changed as well as minor shifts in the resonance frequency.

In agreement with our numerical analysis, Figs. 4–6 clearly show that at each of the transmission minima, there are strong discontinuous features in the optical activity. Although the multiple features in the crosses and arrows are outside of our experimentally measurable range, the arcs show that the frequencies of minimum transmission approach each other as the optical activity increases. Furthermore, it can be seen that the shallower transmission minima correspond to more broadband contributions of the

TABLE II. Summary of optical activity values of the simulated crosses and arrows structures shown in Fig. 2 and the realistic simulated structures presented in Sec. V. The slight changes between the structures shifted the resonance frequencies slightly as well as altered the amount of optical activity. The symbol (*) represents the experimental results of the arcs structure, see the Supplemental Material [25].

Structure	Frequency	Φ ideal (deg)	Frequency	Φ real (deg)
Crosses	0.91	12.08	0.93	8.8
Arrows	1.24	13.19	1.20	12.5
Arcs	1.7	29.8	*	*

Blaschke phase terms due to the increase in the imaginary part of the zero of transmission.

VI. CONCLUSION

We study theoretically and experimentally the optical activity in chiral metamaterial structures based on planar metallic components coupled to their twisted Babinet complements. We show that in chiral metamaterials with low dissipative losses, the Blaschke phase plays a key role in the optical activity, dominating the contributions related to circular dichroism through the Kramers-Kronig relations. We design, fabricate, and measure three designs of chiral metamaterials operating at terahertz frequencies. All three structures show dispersionless optical activity around the resonant transmission peaks, and the difference in performance can be understood from the change of Blaschke phase. For future study, it will be particularly useful to develop an intuitive physical model to understand the relation between geometry and Blaschke phase.

ACKNOWLEDGMENTS

This work is supported by the Australian Research Council via the Centre of Excellence (CUDOS Grant No. CE110001018), and Discovery Projects.

[1] Michael Wiltshire, in *Metamaterials and Plasmonics: Fundamentals, Modelling, Applications*, edited by Sad Zouhdi, Ari Sihvola, and Alexey P. Vinogradov, NATO Science for Peace and Security Series B: Physics and Biophysics (Springer, Dordrecht, 2009), pp. 191–200.

[2] Jianfeng Wu, Binghao Ng, Haidong Liang, Mark B. H. Breese, Minghui Hong, Stefan A. Maier, Herbert O. Moser, and Ortwin Hess, Chiral Metafoils for Terahertz Broadband High-Contrast Flexible Circular Polarizers, Phys. Rev. Applied **2**, 014005 (2014).

[3] S. Tretyakov, A. Sihvola, and L. Jylh, Backward-wave regime and negative refraction in chiral composites, Photonics Nanostruct. Fundam. Appl. **3**, 107 (2005).

[4] Justyna K. Gansel, Martin Wegener, Sven Burger, and Stefan Linden, Gold helix photonic metamaterials: A numerical parameter study, Opt. Express **18**, 1059 (2010).

[5] J. B. Pendry, A chiral route to negative refraction, Science **306**, 1353 (2004).

[6] E. Plum, V. A. Fedotov, A. S. Schwanecke, N. I. Zheludev, and Y. Chen, Giant optical gyrotropy due to electromagnetic coupling, Appl. Phys. Lett. **90**, 223113 (2007).

[7] Yuri Svirko, Nikolay Zheludev, and Michail Osipov, Layered chiral metallic microstructures with inductive coupling, Appl. Phys. Lett. **78**, 498 (2001).

[8] Kirsty Hannam, David A. Powell, Ilya V. Shadrivov, and Yuri S. Kivshar, Dispersionless optical activity in metamaterials, Appl. Phys. Lett. **102**, 201121 (2013).

[9] Kirsty Hannam, David A. Powell, Ilya V. Shadrivov, and Yuri S. Kivshar, Broadband chiral metamaterials with large optical activity, Phys. Rev. B **89**, 125105 (2014).

[10] Zhaofeng Li, Humeyra Caglayan, Evrim Colak, Jiangfeng Zhou, Costas M. Soukoulis, and Ekmel Ozbay, Coupling effect between two adjacent chiral structure layers, Opt. Express **18**, 5375 (2010).

[11] Zhaofeng Li, Kamil Boratay Alici, Evrim Colak, and Ekmel Ozbay, Complementary chiral metamaterials with giant optical activity and negative refractive index, Appl. Phys. Lett. **98**, 161907 (2011).

[12] Zhaofeng Li, Mehmet Mutlu, and Ekmel Ozbay, Chiral metamaterials: From optical activity and negative refractive index to asymmetric transmission, J. Opt. **15**, 023001 (2013).

[13] A. V. Rogacheva, V. A. Fedotov, A. S. Schwanecke, and N. I. Zheludev, Giant Gyrotropy Due to Electromagnetic-Field Coupling in a Bilayered Chiral Structure, Phys. Rev. Lett. **97**, 177401 (2006).

[14] Weiren Zhu, Ivan D. Rukhlenko, Yongjun Huang, Guangjun Wen, and Malin Premaratne, Wideband giant optical activity and negligible circular dichroism of near-infrared chiral metamaterial based on a complementary twisted configuration, J. Opt. **15**, 125101 (2013).

[15] Bingnan Wang, Jiangfeng Zhou, Thomas Koschny, Maria Kafesaki, and Costas M. Soukoulis, Chiral metamaterials: Simulations and experiments, J. Opt. A **11**, 114003 (2009).

[16] M. Decker, M. Ruther, C. E. Kriegler, J. Zhou, C. M. Soukoulis, S. Linden, and M. Wegener, Strong optical activity from twisted-cross photonic metamaterials, Opt. Lett. **34**, 2501 (2009).

[17] H.-T. Chen, J. F. O'Hara, A. K. Azad, and A. J. Taylor, Manipulation of terahertz radiation using metamaterials, Laser Photonics Rev. **5**, 513 (2011).

[18] Jianfeng Dong, Jiangfeng Zhou, Thomas Koschny, and Costas Soukoulis, Bi-layer cross chiral structure with strong optical activity and negative refractive index, Opt. Express **17**, 14172 (2009).

[19] Mingkai Liu, David A. Powell, Ilya V. Shadrivov, and Yuri S. Kivshar, Optical activity and coupling in twisted dimer meta-atoms, Appl. Phys. Lett. **100**, 111114 (2012).

[20] Y. Zhao, M. A. Belkin, and A. Alù, Twisted optical metamaterials for planarized ultrathin broadband circular polarizers, Nat. Commun. **3**, 870 (2012).

[21] Lauren Barr, Ana Díaz-Rubio, Ben Tremain, Jorge Carbonell, Sánchez-Dehesa, José Euan Hendry, and Alastair Hibbins, On the origin of pure optical rotation in twisted-cross metamaterials, Sci. Rep. **6**, 30307 (2016).

[22] Maxim Gorkunov, Vladimir Dmitrienko, Alexander Ezhov, Vladimir Artemov, and Oleg Rogov, Implications of the causality principle for ultra chiral metamaterials, Sci. Rep. **5**, 9273 (2015).

[23] Valerio Lucarini, Jarkko J. Saarinen, Kai-Erik Peiponen, and Erik M. Vartiainen, *Kramers-Kronig Relations in Optical Materials Research* (Springer Science & Business Media, New York, 2005), Vol. 110.

[24] V. V. Ivanov, in *The Theory of Approximate Methods and Their Application to the Numerical Solution of Singular Integral Equations*, edited by P. Noordhoff (Springer, Leyden, New York, 1976).

[25] See the Supplemental Material at http://link.aps.org/supplemental/10.1103/PhysRevApplied.8.014019 for experimental cross-polarization measurements of the crosses structure and the experimental results of the arcs structure.